Original Article

Regions of Low Endothelial Shear Stress Colocalize With Positive Vascular Remodeling and Atherosclerotic Plaque Disruption

An In Vivo Magnetic Resonance Imaging Study

Alkystis Phinikaridou, PhD; Ning Hua, PhD; Tuan Pham, BSc; James A. Hamilton, PhD

Background—Local hemodynamic factors, particularly low endothelial shear stress (ESS), play a role in the focal formation of atherosclerosis. We used in vivo MRI to investigate the role of the magnitude of ESS on vascular remodeling, plaque burden, and disruption using a rabbit model of controlled atherothrombosis.

Methods and Results—Atherosclerosis was induced in New Zealand white rabbits by cholesterol diet and endothelial denudation. MRI was performed before (pretrigger) and after (posttrigger) inducing plaque disruption with Russell viper venom and histamine. Of the 134 vascular segments studied, 28 contained thrombus (disrupted) and 106 did not (nondisrupted). Disrupted plaques were histologically characterized by a thin, inflamed fibrous cap, a dense lipid core, and mural thrombus. Pretriggered MRI revealed that disrupted plaques clustered at regions with low mean ESS (11.55±5.3 versus 20.9±9.74 dynes/cm^2; P<0.001) and low peak ESS (21.5±11.2 versus 49.2±21.5 dynes/cm^2; P<0.001) compared with nondisrupted plaques. The peak ESS negatively correlated with the plaque area (r=−0.56, P<0.001) and remodeling ratio (r=−0.4, P=0.008). There was also a negative correlation between the mean ESS and the remodeling ratio (r=−0.55, P<0.001). Both the peak ESS and the mean ESS did not correlate with the % stenosis; there was a weak but statistically significant correlation with the % cross-sectional narrowing (r=0.3, P=0.002 and r=0.2, P=0.04, respectively). Receiver operating characteristic analysis showed that both mean (Area under the curve =0.78; 95% CI, 0.69–0.87) and peak ESS (Area under the curve=0.85; 95% CI, 0.78–0.93) identified disrupted plaques.

Conclusions—We demonstrated that low ESS is associated with plaque burden, positive vascular remodeling, and plaque disruption in a rabbit model. Assessment of ESS by noninvasive MRI might be useful for assessing atherosclerotic risk. **(*Circ Cardiovasc Imaging*. 2013;6:302-310.)**

Key Words: atherosclerosis ■ endothelial shear stress ■ MRI ■ thrombosis ■ vascular remodeling

Disruption of atherosclerotic plaque and thrombotic occlusion of the lumen is one of the major causes of morbidity and mortality in western societies. Despite the systemic and multifactorial nature of atherosclerosis, plaque development is focal and occurs at particular regions of the vasculature, including the branches, the inner curvature, and the outer wall of bifurcations, where disrupted flow and low endothelial shear stress (ESS) occur.[1] ESS is the tangential stress derived from the friction of flowing blood on the vascular endothelium surface and is expressed as force/unit area (N/m^2 or Pascal or dyne/cm^2). ESS is proportional to the product of the blood viscosity and the spatial gradient of blood velocity at the wall (ESS=dv/dy). ESS is pulsatile with a magnitude that ranges from 15 to 70 dyne/cm^2 over the cardiac cycle and yields a positive time-average.[2–4] The first evidence implicating ESS in the localization of atherosclerosis in humans was described by Caro et al[5] Later, sophisticated computational fluid dynamic simulations in autopsy-based models of human coronary[6] and carotid arteries,[7] and aorta[8] showed that areas with low ESS (10–12 dynes/cm^2) contained atherosclerosis as found at autopsy. Furthermore, plaques found in regions with low ESS were shown to have histological features of plaque vulnerability, including fewer Smooth muscle cells, lesser collagen, more lipids, positive/outward vascular remodeling in mice,[9] and swine[10] models.

Clinical Perspective on p 310

The proatherogenic role of low ESS has been extensively evaluated in vitro,[3,11] and in vivo using Doppler ultrasound in human carotid[7] and murine atherosclerosis,[12,13] using intravascular ultrasound (IVUS) in human coronary[14–16] and swine[10,17] arteries, and using MRI in human carotid[18–20] and thoracic arteries,[21] and murine models.[22] Some of these studies have

Received September 18, 2012; accepted January 14, 2013.

From the Department of Physiology and Biophysics (A.P., N.H., T.P., J.A.H.) and Department of Biomedical Engineering (T.P., J.A.H.), Boston University School of Medicine, Boston, MA. Alkystis Phinikaridou's present affiliation: St Thomas' Hospital, Lambeth Palace Road, London, SE1 7EH.

Guest Editor for this article was David A. Bluemke, MD, PhD.

Correspondence to Dr. James A. Hamilton, 700 Albany St, 3rd Floor, W-302, Department of Physiology and Biophysics, Boston University School of Medicine, Boston, MA 02118. E-mail jhamilt@bu.edu

Circ Cardiovasc Imaging **is available at http://circimaging.ahajournals.org** **DOI: 10.1161/CIRCIMAGING.112.000176**

also provided a link between low ESS and positive vascular remodeling[14–16] or low ESS and histological evidence of plaque instability.[10,12,13,17,18,22] However, only limited studies using invasive IVUS have investigated the association among low ESS, plaque progression, vascular remodeling, and plaque vulnerability, and have tested the feasibility of these measurements to predict plaque growth and instability.[14,23]

MRI has evolved as a noninvasive imaging modality to visualize the vessel wall with high spatial resolution in humans[24–26] and animal models.[27,28] MRI acquisition protocols can also provide velocity data that can be accurately matched with anatomic images. Various flow data can be extracted from the acquired images, including velocity profiles, flow rates, shear rate, and shear stress.[21,29,30]

In this study, we have used in vivo MRI in a rabbit model of atherosclerosis and controlled plaque disruption[31–33] to investigate whether low values of ESS associate with plaque burden, vascular remodeling, and plaque disruption. This model was initially used for the detection of mural thrombus formed after plaque disruption by in vivo MRI without[34] and with a fibrin contrast agent.[35] Most recently, we have shown the histological similarities between rabbit and human plaques,[33] and the ability of in vivo MRI measurements to predict plaque with a higher likelihood of disruption.[28]

Methods

Animal Model

Male New Zealand white rabbits (n=10, Charles River Laboratories, MA) were rendered atherosclerotic as previously described.[28,31–35] Briefly, rabbits were fed a 1% cholesterol diet (PharmaServe, MA) for 2 weeks before and 6 weeks after balloon injury of the abdominal aorta, followed by 4 weeks of normal chow diet. Denudation of the aortic wall was performed under general anesthesia (acepromazine [0.75 mg/kg IM], ketamine [35 mg/kg, IM], and xylazine [2.5 mg/kg, IM]). As in our previously published work, a 3F Fogarty catheter (Edwards Biosciences) was introduced into the aorta through a femoral artery cutdown. The catheter was advanced to the level of the diaphragm, where the balloon was inflated. Then the catheter was gently retracted to the iliofemoral artery. This procedure was performed 3 times in each rabbit. The catheter was then removed, and the incision was closed with sutures. Therefore, the aorta between the renal branches, right below the diaphragm, and the iliac bifurcation was denudated covering a length of ≈9 to 10 cm.[28,31–35]

Pharmacological triggering of thrombosis was induced with Russell viper venom (0.15 mg/kg IP; Enzyme Research, IN), a procoagulant factor followed 30 minutes later by histamine, a vasoconstrictor in rabbits (0.02 mg/kg IV; Sigma-Aldrich, MO). This procedure was performed twice within a 48-hour period. Within 24 hours after the final MRI, the rabbits received heparin (1000 united states pharmacopeia (USP) units IV; Sigma-Aldrich) to prevent postmortem blood clotting and were euthanized with a bolus injection of sodium pentobarbital (100 mg/kg IV). Subsequently, the aortas were excised, stretched to physiological lengths, and fixed in 10% formalin for histological analysis. During extraction, the aortas were marked with suture ligature at distances above and below the left renal branch that matched the total length covered by the in vivo MRI slices. Before cutting the vessel, its total length was measured with a ruler. After extraction, the ligatures were used to reextend the aortas to their physiological length, at which time they were fixed with 10% formalin solution (Thermo Scientific, Waltham, MA) and cut in 1.5- to 2.0-cm segments. To avoid rotational problems, the proximal end of each segment was marked with ink on its anterior side. Animal studies were performed in accordance with guidelines approved by the Institutional Animal Care and Use Committee of Boston University.

MRI Protocol

In vivo MRI experiments were performed on supine rabbits using a 3T Philips Intera Scanner (Philips Medical Systems, OH) and a 6-channel synergy knee coil (Figure 1). A peripheral pulse oximeter was placed on the ear for cardiac gating. The aorta of atherosclerotic rabbits, between the renal branches and the iliac bifurcation, was imaged before (pre) and 48 hours after (post) the first pharmacological triggering. Coronal three-dimensional (3D) phase-contrast magnetic resonance (MR) angiograms acquired with a T1-weighted fast-field echo sequence and Repetition Time (TR) =20 ms, Echo Time (TE) =3 ms, flip angle=15°, Field of View (FOV) =300×150 mm, matrix=256×122, slice thickness=1 mm, in-plane resolution=1.17×1.23 mm, reconstructed resolution=0.6×0.6 mm, slices=20, averages=2, and duration=3 minutes. The maximum intensity projection images were used to plan the subsequent scans. Two-dimensional axial T1-weighted black-blood images were acquired with a double inversion recovery, turbo spin echo sequence, and cardiac gating. The parameters for the T1-weighted black-blood images were as follows: TR=2 seconds, TE=5.4 ms, Turbo Spin Echo (TSE) =6, black-blood pulse=4 mm, delay=350 ms, FOV=120×85 mm, acquired matrix=384×270, slice thickness=4 mm, acquired in-plane resolution=0.31×0.31 mm, reconstructed resolution=0.23×0.23 mm, slices=25, averages=2, and duration=10 to 15 minutes. Cardiac-gated, phase-contrast images were acquired with a 3D T1-weighted fast-field echo sequence. The acquisition parameters were as follows: TR=15.5 ms, TE=6.8 ms, flip angle=15°, slices=25, FOV=50×30 mm, matrix=208×138, slice thickness=4 mm, acquired in-plane resolution=0.24×0.22 mm, reconstructed resolution=0.2×0.2 mm, encoding velocity=150 cm/s, cardiac phases=8 to 10, averages=2, and scan duration=10 minutes. Finally, contrast-enhanced (Magnevist 0.1 mmol/kg, IV) phase-contrast MR angiogram images were acquired 2 to 3 minutes after injection of the contrast agent, with the same parameters described above but without cardiac gating.

Histology

Transverse cryo-sections (10 μm) were collected throughout the length of each segment, at 500-μm intervals, and stained with Masson's trichrome (Sigma-Aldrich) for plaque components and thrombus. Unstained sections were used for polarized light microscopy to identify the lipids. Disrupted (vulnerable) plaques were defined as those with attached platelet and fibrin-rich thrombus, whereas plaques without overlying thrombus were defined as nondisrupted (stable).[28,33–35] The distances from the aortic renal branches and the iliac bifurcation were used as internal anatomic markers to match the MRI and histological sections.

Image Analysis

Pretriggered MRI images were used to calculate the plaque, vessel, and lumen areas, % cross-sectional narrowing, % stenosis, ESS,

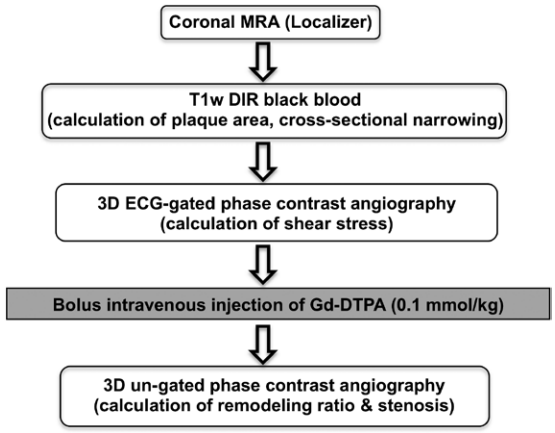

Figure 1. In vivo MRI acquisition protocol and data analysis. MRA indicates magnetic resonance angiogram; T1w DIR, T1-weighted double inversion recovery; and 3D, three-dimensional.

and arterial remodeling as previously described.[28] The posttriggered MRI were used to detect thrombus and classify plaques as nondisrupted or disrupted. In all the cases, the final categorization of disrupted or nondisrupted plaques was performed on the basis of histology. T1-weighted black-blood images were used to calculate the plaque area (PA) and the % cross-sectional narrowing by manually segmenting the adventitial and luminal contours of the vessel wall as follows:

$$Plaque\ area = Vessel\ area - Lumen\ area;$$

$$CSN = \frac{Plaque\ area}{Vessel\ area} \times 100.$$

The cardiac-gated phase-contrast MR angiogram images were used to calculate the ESS (dynes/cm^2) using an in-house Matlab software. The lumen was automatically segmented using a level set function. The vessel wall was divided into 16 segments, which were determined at every 22.5° in the circumferential direction from the center of the mass. By averaging the cardiac cycle, the time-averaged shear rates for 16 segments were calculated, the maximum of which was defined as the peak shear rate, whereas the mean was determined as the mean shear rate. The ESS was calculated as: shear rate×viscosity (4 cP).[21]

Ungated 3D phase-contrast MR angiogram images acquired immediately after injection of gadolinium-diethylenetriaminepentacetate (Gd-DTPA) were used to calculate the remodeling ratio (RR) and the % stenosis as previously described.[28] Briefly, the anatomic images were used to measure the vessel area for the calculation of the RR, and the corresponding flow-encoded images were used to calculate the lumen area and the % stenosis. The RR and the % stenosis were calculated after correcting for arterial tapering and for interindividual variability of arterial size. The RR was calculated as follows:

$$RR = \frac{Vessel\ area_{lesion}}{Vessel\ area_{reference}}.$$

Three remodeling categories defined as previously described[28,36]: positive if RR>1.05, intermediate if 0.95≤RR≤1.05, and negative if RR<0.95. The % stenosis is calculated as

$$\%\ Stenosis = 1 - \left[\frac{Lumen\ area_{lesion}}{Lumen\ area_{reference}}\right] \times 100.$$

Because of diffuse vessel wall disease in this animal model, the reference site was chosen to be the slice with the least amount of plaque, assuming that it was least affected by the disease.

Statistical Analysis

Analyses were performed using SPSS 11.0 (SPSS Inc). For 2-group comparisons, continuous variables were compared using either a 2-sample *t* test or a Mann–Whitney nonparametric test. Categorical variables were compared using the χ^2 test. Multiple group comparisons were done using 1-way ANOVA followed by the Bonferroni post hoc test. Qualitative data are presented as frequencies. Receiver operating characteristic (ROC) curves of the MRI measurements were also calculated. The cutoff values for the mean ESS=12.63 dyne/cm^2 and peak ESS=39.45 dyne/cm^2 were calculated on the basis of ROC curve as the value corresponding to the highest sensitivity and specificity in predicting plaque disruption. Data are presented as mean±SD. $P<0.05$ were used to define statistical significance.

Results

Atherosclerotic Plaque Disruption Occurs at Vascular Regions With Low ESS Undergoing Positive Remodeling

Atherosclerosis was observed in all rabbits, and thrombosis occurred in 6/10 (60%) of the animals. A total of 134 atherosclerotic wall segments/slices were analyzed, of which 28 (20.8%) showed mural thrombus after triggering for plaque disruption, whereas 106 did not (79.1%).

An example of the association among the mean magnitude of ESS, vascular remodeling, and plaque disruption after triggering is illustrated in Figure 2. The pretrigger T1-weighted black-blood images (Figure 2A and 2F) compare a nondisrupted and a disrupted plaque, respectively. The pretrigger flow-compensated images (Figure 2B and 2G) used to calculate the RR show that the nondisrupted plaque had undergone negative remodeling (RR=0.85), whereas the disrupted plaque had undergone positive remodeling (RR=1.17). The pretrigger flow-encoded images (Figure 2C and 2H) were used to derive the vectors associated with the magnitude of the mean ESS at

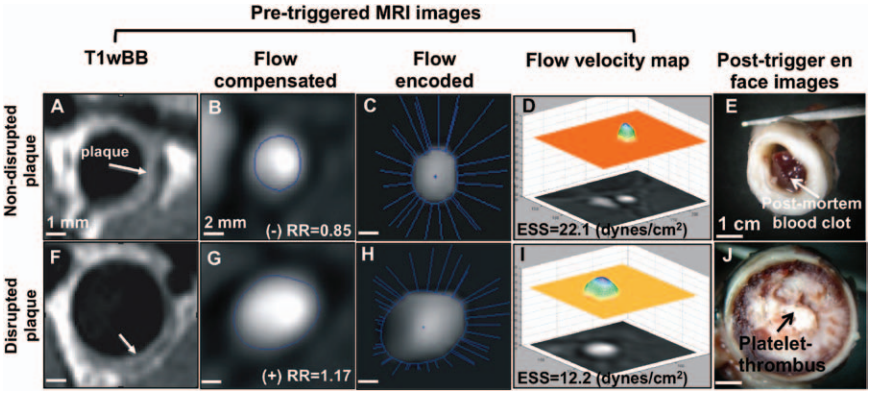

Figure 2. Atherosclerotic plaque disruption occurs at regions with low endothelial shear stress (ESS) undergoing positive vascular remodeling. Pretrigger T1-weighted black-blood (T1wBB) images show the vessel wall thickening at a site of (**A**) a nondisrupted and (**F**) a disrupted plaque. Corresponding flow-compensated images show the constriction of the vessel wall at the site of the nondisrupted plaque (**B**) and the expansion/positive remodeling of the vessel wall at the site of plaque disruption (**G**). **C** and **H**, Flow-encoded images used to calculate the magnitude of the ESS. Each line means the ESS was calculated at that specific point perpendicular to the circumference of the vessel wall. The length of the line indicates the absolute magnitude of the value of shear rate. When the line is pointing outward, it means that the shear rate is positive, whereas when the line is pointing inward it means that the shear rate is negative. Corresponding velocity maps show the localization of the nondisrupted plaque (**D**) at a region with higher mean ESS compared with the disrupted plaque (**I**). Ex vivo en face images taken after triggering for plaque disruption show the presence of a platelet-rich thrombus at the site of plaque disruption (**E**) and the expansion of the vessel wall (**J**). Conversely, the nondisrupted plaque undergoes negative remodeling (**E**). RR indicates remodeling ratio.

the wall contours (Figure 2B and 2G). The magnitude of the ESS is illustrated on the surface plots (Figure 2D and 2I) that indicate a higher mean ESS (22.1 dynes/cm^2) at the site of the nondisrupted plaque and a lower mean ESS (12.2 dynes/cm^2) at the site of plaque disruption. Ex vivo en face images verified the constrictive remodeling at the site of the nondisrupted plaque (Figure 2E) and the expansion of the vessel wall at the site of plaque disruption (Figure 2J). Furthermore, Figure 2J reveals occlusive platelet-rich thrombus associated with plaque disruption, whereas the clot seen at the site of the nondisrupted plaque is coagulated blood.

Another example of the association among vascular remodeling, ESS, and histological characteristics of plaque vulnerability is demonstrated in Figure 3. A nondisrupted plaque (Figure 3A–3F) with negative remodeling (Figure 3B) located in a region of relatively high mean (18.3 dynes/cm^2) and high peak ESS (87.1 dynes/cm^2) was characterized by proliferating SMC and proteoglycans (Figure 3C and 3E) and low-lipid content (Figure 3D and 3F). Conversely, a disrupted plaque (Figure 3G–3L) with positive remodeling (Figure 3H) located in a region of low mean (12.6 dynes/cm^2) and low peak (28.2 dynes/cm^2) ESS was histologically characterized by a thin fibrous cap, which became discontinuous at the site of plaque rupture (Figure 3I and 3K), and a dense lipid core (Figure 3J and 3L).

Statistical analysis of disrupted and nondisrupted plaques revealed that disrupted plaques localize at regions with low mean ESS (11.55±5.3 versus 20.9±9.74; P<0.001) and low peak ESS (21.5±11.2 versus 49.2±21.5; P<0.001) compared with nondisrupted plaques (Table).

Association of the Magnitude of ESS With Plaque Characteristics Measured In Vivo

The association of the magnitude of ESS, plaque characteristics, and vascular remodeling is illustrated in Figure 4. The peak ESS negatively correlated with the PA (r=–0.56, P<0.001) and RR (r=–0.4, P=0.008), indicating that large plaques and positive arterial remodeling occurred in regions with low ESS. There was also a strong negative correlation between the mean ESS and the RR (r=–0.55, P<0.001) but not with the PA. As in the case of the peak ESS, the mean ESS did not correlate with the % stenosis. Finally, both the peak ESS and the mean ESS correlated weakly but significantly with the % cross-sectional narrowing (r=0.3, P=0.002 and r=0.2, P=0.04, respectively).

Association of the Magnitude of ESS With Vascular Remodeling

The association between the magnitude of local ESS and the type of vascular remodeling is demonstrated in Figure 5. Positive remodeling was seen in regions of both lower mean ESS (Figure 5A) and lower peak ESS (Figure 5B), whereas negative remodeling occurred in regions with higher mean and higher peak ESS. The peak ESS was distinctively different among the different vascular remodeling types (P<0.001) compared with the mean ESS.

Association of the Magnitude of ESS With Disrupted Plaque

The discrimatory power of ESS in identifying disrupted plaque was studied using ROC analysis (Figure 6A). Both low mean ESS (AUC=0.78; 95% CI, 0.69–0.87) and low peak ESS (AUC=0.85; 95% CI, 0.78–0.93) showed a moderate discriminatory power and, therefore, potential utility as a diagnostic test in determining disrupted from nondisrupted plaque. Furthermore, ROC analysis revealed the best cutoff value for the mean ESS=12.63 dynes/cm^2 and for the peak ESS=39.45 dynes/cm^2. Classification of ESS shows that 66.6% of disrupted plaques had a mean ESS<12.63 dynes/cm^2 and 96.4% had a peak

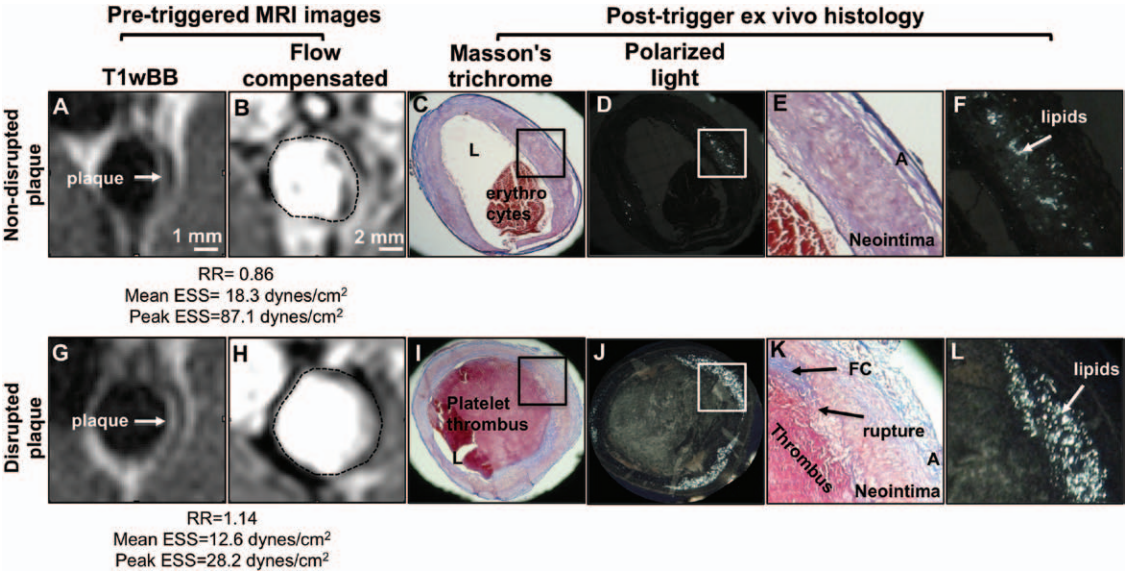

Figure 3. Plaques found at regions of low endothelial shear stress (ESS) and positive remodeling have histological characteristics of plaque vulnerability. Pretrigger T1-weighted black-blood (T1wBB) images show the vessel wall thickening at a site of a nondisrupted (**A**) and a disrupted plaque (**G**). Corresponding flow-compensated images show negative remodeling for the nondisrupted (**B**) and positive remodeling for the disrupted plaque (**H**). **C** and **I**, **E** and **K**, Lower and higher magnification Masson's trichrome staining reveal the thrombus and the site of fibrous cap rupture (**K**). **D** and **F**, **J** and **L**, Lower and higher magnification polarized light microscopy reveal a lipid-poor nondisrupted plaque and a lipid-rich disrupted plaque, respectively. Lipids are in contact with the thrombus at the site of rupture (**L**). FC indicates fibrous cap; and RR, remodeling ratio.

Table. Plaque Disruption Occurs Within Regions of Low ESS

Measurement	Nondisrupted Plaque (n=106)	Disrupted Plaque (n=28)	*P*
Mean ESS, dynes/cm^2	20.9±9.74	11.5±5.3	<0.001
Peak ESS, dynes/cm^2	49.2±21.5	21.5±11.2	<0.001

ESS indicates endothelial shear stress.

ESS<39.45 dynes/cm^2 (Figure 6B). Conversely, only 33.4% of the disrupted plaques had mean ESS>12.63 dynes/cm^2 and 3.6% had a peak ESS>39.4 dynes/cm^2. Of the non-disrupted plaques, only 21.7% had a mean peak ESS<12.63 dynes/cm^2 and 41% had a peak ESS<39.45 dynes/cm^2 (Figure 6C).

Discussion

In this study, we used a rabbit model of accelerated atherosclerosis and controlled plaque disruption to study the relationship of ESS with plaque burden, vascular remodeling, and plaque disruption. Previous studies have highlighted low ESS as a critically important determinant of plaque development and progression to high-risk (vulnerable) plaques with a large necrotic core, increased inflammation, and thin fibrous cap. All these histological features are replicated in disrupted aortic plaques in the rabbit model. Moreover, the ability to experimentally induce plaque disruption and thrombosis at a precise time point provides a functional end point to classify plaque as nondisrupted/stable (no thrombus) or disrupted/vulnerable (mural thrombus). Using MRI protocols that previously demonstrated a strong association among plaque burden, positive remodeling, and plaque disruption,[28] we now tested the association of ESS with plaque burden, vascular remodeling, and the likelihood of plaque disruption.

Using noninvasive in vivo MRI, we found that regions of low local ESS associated with larger PA, positive arterial remodeling, and plaque disruption. Both the peak ESS and the mean ESS correlated weakly but significantly with the % cross-sectional narrowing, but because of the vascular remodeling effect there was no association of ESS with % stenosis. Classification of ESS showed that the majority of the disrupted plaques occurred in regions with mean ESS<12.63 dynes/cm^2 and with peak ESS<39.45 dynes/cm^2. Finally, ROC analysis showed that both mean ESS and peak ESS have a moderate discrimatory power in identifying disrupted plaques. These data suggest that local ESS might be critical for plaque burden and disruption and that noninvasive assessment of ESS may be a useful surrogate marker for stratifying atherosclerotic risk.

Positive remodeling delays the development of flow-limiting stenosis by preserving the lumen as seen in histological[37] and in vivo imaging studies.[38–40] Despite the initial beneficial role of outward remodeling, it also increases the likelihood of plaque destabilization, rupture, and clinical symptoms. Recently, 3 prospective clinical studies using IVUS and CT have shown that a large plaque burden, the presence of thin-cap fibroatheromas (Predictors of Response to CRT [PROSPECT] study),[41] a positive remodeling index (VH-IVUS in Vulnerable Atherosclerosis [VIVA] study),[42] and a positive remodeling together with low attenuation on CT[43] were predictors of adverse cardiac events in humans with coronary artery disease. In vivo IVUS studies have shown that high-risk swine coronary plaques[10,23] and human coronary arteries exhibiting

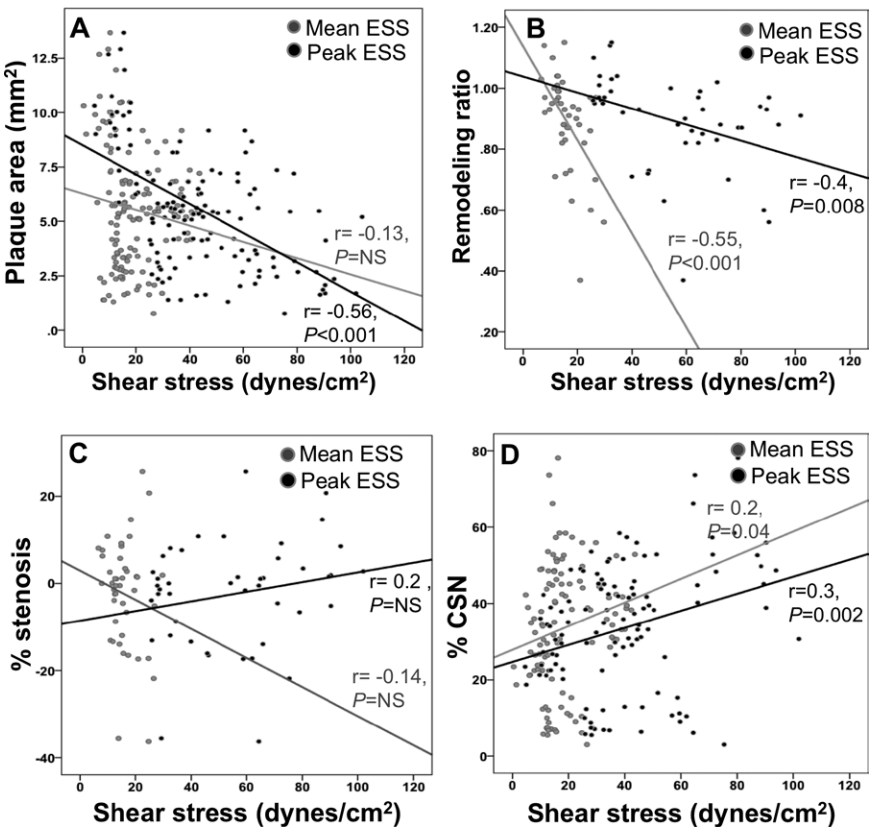

Figure 4. Association of endothelial shear stress (ESS) with plaque characteristics and vascular remodeling. The peak ESS correlates negatively with the plaque area (**A**) and remodeling ratio (**B**) indicating that large plaques and positive arterial remodeling develop in regions of low ESS. The mean ESS correlates with the remodeling ratio. Both peak and mean ESS do not correlate with the % stenosis (**C**), but there was a weak but statistically significant correlation with the % cross-sectional narrowing (r=0.3, P=0.002 and r=0.2, P=0.04, respectively; **D**).

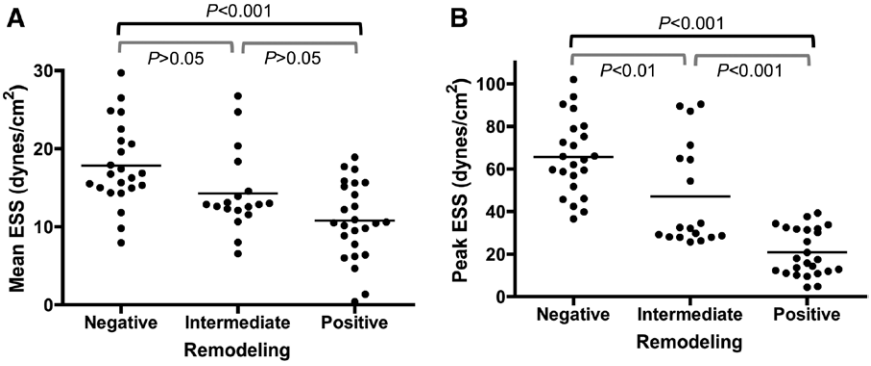

Figure 5. Local endothelial shear stress (ESS) correlates with the type of vascular remodeling. **A**, Mean ESS is statistically lower in plaques undergoing positive vascular remodeling. **B**, Peak ESS is significantly lower in plaques undergoing intermediate and positive remodeling compared with those undergoing negative remodeling.

progression and in-stent restenosis[14] localize at regions of low ESS (<10 dynes/cm^2). Positive remodeling requires restructuring of the extracellular matrix scaffold to release their imposed constraints, which could be promoted by increased secretion of matrix metalloproteinases[44] that degrade the extracellular matrix. Moreover, augmented expression and activity of extracellular matrix-degrading enzymes were shown to occur in regions of low ESS and colocalize with thin fibrous cap atheromas in swine.[17]

Previous studies have identified hemodynamic shear stress as an important determinant of endothelial function and phenotype. Arterial shear stress (>15 dyne/cm^2) induces endothelial quiescence and an atheroprotective gene expression profile, whereas low shear stress (<4 dyne/cm^2) that is prevalent at atherosclerosis-prone sites stimulates an atherogenic phenotype.[11] Although it is generally assumed that the average ESS over the cardiac cycle in large straight arteries experiencing laminar flow remains at a physiological level of ≈15 to 20 dynes/cm^2, the value of ESS varies within the arterial tree and is inversely related to vessel diameter and species size.[45] Similar to our data and despite the interspecies differences in the absolute ESS values, low in vivo ESS has been found in (1) mice upstream of a cast, placed to cause vessel obstruction, at the position where plaques with vulnerable histological features develop (112±52 dynes/cm^2),[22] as measured by MRI; (2) high-risk swine coronary arteries (<10 dynes/cm^2), as measured by IVUS[10,23]; and (3) human coronary arteries exhibiting progression and in-stent restenosis (<9.1 dynes/cm^2), as measured by IVUS.[14]

Because plaque disruption is a complex process, comprehensive plaque vulnerability assessment should involve a combination of systemic markers, plaque morphological features, hemodynamic conditions, and biomechanical factors. Technological advances in MRI, image processing software, and development of molecular imaging agents have improved the characterization and measurement of most of these parameters and provide a promising tool for the noninvasive assessment of atherosclerotic disease. MRI sequences that allow velocity mapping of the coronary arteries[46,47] are now available and could be used for the calculation of ESS in the coronary tree.

Study Limitations

Although no animal model is expected to exhibit all features of human atherosclerosis and plaque rupture, the rabbit model has many similarities, including 6 well-characterized stages of human plaques.[33] In addition, we[33] and others[31,32] have shown that rabbit disrupted plaques are histologically characterized by large PA, thin fibrous cap, dense lipid core, increased inflammatory infiltrate, neovascularization, tissue necrosis, media, and adventitial disorganization, all of which are features of plaque vulnerability in humans.

Although the rabbit model offers thrombosis as an end point to classify plaque, it is important to consider how the pharmacologically induced plaque rupture corresponds to plaque rupture in humans. As shown by us[33] and others,[31,32] thrombosis in the rabbit is not an unspecific event, but it occurs only in plaques that share several well-established histological features of plaque vulnerability as those described in humans. Precisely what triggers human plaque to disrupt remains unknown. Studies of coronary arteries[48] have suggested that it involves platelet activation and adhesion, and the release of vasoconstriction molecules, including thromboxane A2 and serotonin. Therefore, the combination of a procoagulant factor (viper venom) and a vasoconstriction agent (histamine) may be an acceptable physiological approximation.

A technical limitation of this work is that the ESS was calculated using velocity data encoded in only the foot to head direction. This could introduce errors in the measurement of ESS if the MRI slices were not perfectly perpendicular to the vessel wall and the direction of blood flow. Another limitation of this study was that data acquisition and analysis were performed at a single time point. Therefore, the role of ESS in the natural progression of atherosclerosis and whether it is a causative or associative factor in the development of atherosclerosis could not be assessed. Such conclusions require a longitudinal study that is the subject of ongoing research in our laboratory.

This rabbit model yielded generally similar conclusions as recent studies with swine coronary arteries, which have good correlations with findings in human coronaries, despite the lack of intraplaque hemorrhage and calcification in the rabbit plaques. However, the role of ESS in carotid atherosclerosis has yielded inconclusive results and so far some studies showed a negative correlation between vessel wall thickness and average shear stress,[18] whereas others show a positive correlation.[49] Similarly, some carotid MRI studies have shown plaque ulceration at regions of high ESS, where the plaque protrudes into the lumen,[50] whereas others have shown that higher critical plaque wall stress values are more closely associated with plaque rupture than critical flow shear stress.[51]

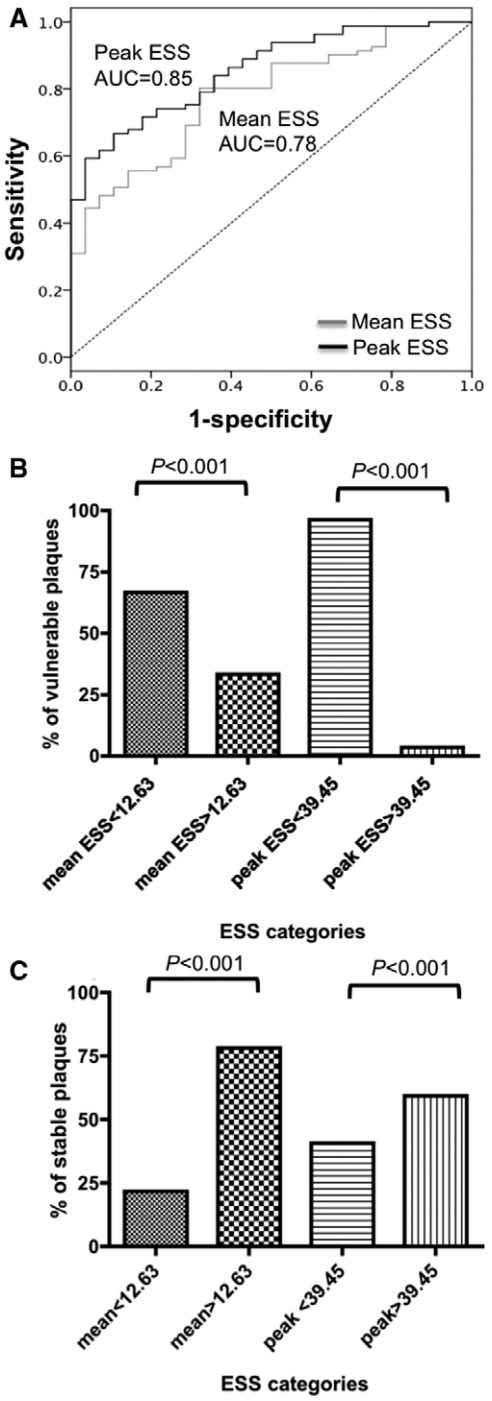

Figure 6. Low local endothelial shear stress (ESS) correlates with the plaque vulnerability. **A**, Receiver operating characteristic (ROC) analysis shows that both mean and peak ESS have a moderate discrimatory power in identifying vulnerable plaque. **B**, Classification of ESS shows that 66.6% of the plaques that disrupt had a mean peak ESS<12.63 dynes/cm^2 and 96.4% had a peak ESS <39.45 dynes/cm^2. **C**, Classification of ESS shows that only 21.7% of the plaques that did not disrupt had a mean peak ESS <12.63 dynes/cm^2 and 41% had a peak ESS<39.45 dynes/cm^2. AUC indicates area under the curve.

Conclusions

Using a rabbit model of controlled atherothrombosis, we demonstrated that low ESS is associated with increased plaque burden, positive arterial remodeling, and plaque disruption after pharmacological triggering. Assessment of ESS by noninvasive MRI in individuals with atherosclerotic disease might be a promising measurement to study plaque growth and atherosclerotic risk. Despite the high predictive value of low ESS in detecting plaque disruption in this animal model, larger scale longitudinal studies in other animal models and humans, and at different sites of the vasculature are needed to establish the role of ESS in plaque progression and whether it is a suitable quantitative marker of plaque vulnerability.

Acknowledgments

We thank Dr Alexandros Tzatsos for helpful comments during the preparation of this manuscript.

Sources of Funding

This project was supported by National Institustes of Health Grant 5P50HL083801 (Dr Hamilton).

Disclosures

Dr Hamilton has equity in a company vascuVis that could commercialize the technology. Boston University has filed a patent application on technology related to the article.

References

1. Wentzel JJ, Chatzizisis YS, Gijsen FJ, Giannoglou GD, Feldman CL, Stone PH. Endothelial shear stress in the evolution of coronary atherosclerotic plaque and vascular remodelling: current understanding and remaining questions. *Cardiovasc Res*. 2012;96:234–243.
2. Malek AM, Alper SL, Izumo S. Hemodynamic shear stress and its role in atherosclerosis. *JAMA*. 1999;282:2035–2042.
3. Gimbrone MA Jr, Topper JN, Nagel T, Anderson KR, Garcia-Cardeña G. Endothelial dysfunction, hemodynamic forces, and atherogenesis. *Ann N Y Acad Sci*. 2000;902:230–239; discussion 239.
4. Stone PH, Coskun AU, Yeghiazarians Y, Kinlay S, Popma JJ, Kuntz RE, Feldman CL. Prediction of sites of coronary atherosclerosis progression: *in vivo* profiling of endothelial shear stress, lumen, and outer vessel wall characteristics to predict vascular behavior. *Curr Opin Cardiol*. 2003;18:458–470.
5. Caro CG, Fitz-Gerald JM, Schroter RC. Arterial wall shear and distribution of early atheroma in man. *Nature*. 1969;223:1159–1160.
6. Asakura T, Karino T. Flow patterns and spatial distribution of atherosclerotic lesions in human coronary arteries. *Circ Res*. 1990;66:1045–1066.
7. Ku DN, Giddens DP, Zarins CK, Glagov S. Pulsatile flow and atherosclerosis in the human carotid bifurcation. Positive correlation between plaque location and low oscillating shear stress. *Arteriosclerosis*. 1985;5:293–302.
8. Moore JE Jr, Xu C, Glagov S, Zarins CK, Ku DN. Fluid wall shear stress measurements in a model of the human abdominal aorta: oscillatory behavior and relationship to atherosclerosis. *Atherosclerosis*. 1994;110:225–240.
9. Cheng C, Tempel D, van Haperen R, van der Baan A, Grosveld F, Daemen MJ, Krams R, de Crom R. Atherosclerotic lesion size and vulnerability are determined by patterns of fluid shear stress. *Circulation*. 2006;113:2744–2753.
10. Chatzizisis YS, Jonas M, Coskun AU, Beigel R, Stone BV, Maynard C, Gerrity RG, Daley W, Rogers C, Edelman ER, Feldman CL, Stone PH. Prediction of the localization of high-risk coronary atherosclerotic plaques on the basis of low endothelial shear stress: an intravascular ultrasound and histopathology natural history study. *Circulation*. 2008;117:993–1002.
11. Malek AM, Alper SL, Izumo S. Hemodynamic shear stress and its role in atherosclerosis. *JAMA*. 1999;282:2035–2042.
12. Cheng C, Tempel D, van Haperen R, van der Baan A, Grosveld F, Daemen MJ, Krams R, de Crom R. Atherosclerotic lesion size and vulnerability are determined by patterns of fluid shear stress. *Circulation*. 2006;113:2744–2753.
13. Cheng C, Tempel D, van Haperen R, de Boer HC, Segers D, Huisman M, van Zonneveld AJ, Leenen PJ, van der Steen A, Serruys PW, de Crom R, Krams R. Shear stress-induced changes in atherosclerotic plaque

composition are modulated by chemokines. *J Clin Invest*. 2007;117:616–626.
14. Stone PH, Coskun AU, Kinlay S, Clark ME, Sonka M, Wahle A, Ilegbusi OJ, Yeghiazarians Y, Popma JJ, Orav J, Kuntz RE, Feldman CL. Effect of endothelial shear stress on the progression of coronary artery disease, vascular remodeling, and in-stent restenosis in humans: *in vivo* 6-month follow-up study. *Circulation*. 2003;108:438–444.
15. Stone PH, Coskun AU, Kinlay S, Popma JJ, Sonka M, Wahle A, Yeghiazarians Y, Maynard C, Kuntz RE, Feldman CL. Regions of low endothelial shear stress are the sites where coronary plaque progresses and vascular remodelling occurs in humans: an *in vivo* serial study. *Eur Heart J*. 2007;28:705–710.
16. Wentzel JJ, Janssen E, Vos J, Schuurbiers JC, Krams R, Serruys PW, de Feyter PJ, Slager CJ. Extension of increased atherosclerotic wall thickness into high shear stress regions is associated with loss of compensatory remodeling. *Circulation*. 2003;108:17–23.
17. Chatzizisis YS, Baker AB, Sukhova GK, Koskinas KC, Papafaklis MI, Beigel R, Jonas M, Coskun AU, Stone BV, Maynard C, Shi GP, Libby P, Feldman CL, Edelman ER, Stone PH. Augmented expression and activity of extracellular matrix-degrading enzymes in regions of low endothelial shear stress colocalize with coronary atheromata with thin fibrous caps in pigs. *Circulation*. 2011;123:621–630.
18. Tang D, Yang C, Mondal S, Liu F, Canton G, Hatsukami TS, Yuan C. A negative correlation between human carotid atherosclerotic plaque progression and plaque wall stress: *in vivo* MRI-based 2D/3D FSI models. *J Biomech*. 2008;41:727–736.
19. Markl M, Wegent F, Zech T, Bauer S, Strecker C, Schumacher M, Weiller C, Hennig J, Harloff A. *In vivo* wall shear stress distribution in the carotid artery: effect of bifurcation geometry, internal carotid artery stenosis, and recanalization therapy. *Circ Cardiovasc Imaging*. 2010;3:647–655.
20. Harloff A, Nussbaumer A, Bauer S, Stalder AF, Frydrychowicz A, Weiller C, Hennig J, Markl M. *In vivo* assessment of wall shear stress in the atherosclerotic aorta using flow-sensitive 4D MRI. *Magn Reson Med*. 2010;63:1529–1536.
21. Wentzel JJ, Corti R, Fayad ZA, Wisdom P, Macaluso F, Winkelman MO, Fuster V, Badimon JJ. Does shear stress modulate both plaque progression and regression in the thoracic aorta? Human study using serial magnetic resonance imaging. *J Am Coll Cardiol*. 2005;45:846–854.
22. van Bochove GS, Straathof R, Krams R, Nicolay K, Strijkers GJ. MRI-determined carotid artery flow velocities and wall shear stress in a mouse model of vulnerable and stable atherosclerotic plaque. *MAGMA*. 2010;23:77–84.
23. Koskinas KC, Feldman CL, Chatzizisis YS, Coskun AU, Jonas M, Maynard C, Baker AB, Papafaklis MI, Edelman ER, Stone PH. Natural history of experimental coronary atherosclerosis and vascular remodeling in relation to endothelial shear stress: a serial, *in vivo* intravascular ultrasound study. *Circulation*. 2010;121:2092–2101.
24. Botnar RM, Stuber M, Kissinger KV, Kim WY, Spuentrup E, Manning WJ. Noninvasive coronary vessel wall and plaque imaging with magnetic resonance imaging. *Circulation*. 2000;102:2582–2587.
25. Fayad ZA, Fuster V, Fallon JT, Jayasundera T, Worthley SG, Helft G, Aguinaldo JG, Badimon JJ, Sharma SK. Noninvasive *in vivo* human coronary artery lumen and wall imaging using black-blood magnetic resonance imaging. *Circulation*. 2000;102:506–510.
26. Yuan C, Mitsumori LM, Ferguson MS, Polissar NL, Echelard D, Ortiz G, Small R, Davies JW, Kerwin WS, Hatsukami TS. *In vivo* accuracy of multispectral magnetic resonance imaging for identifying lipid-rich necrotic cores and intraplaque hemorrhage in advanced human carotid plaques. *Circulation*. 2001;104:2051–2056.
27. Steen H, Lima JA, Chatterjee S, Kolmakova A, Gao F, Rodriguez ER, Stuber M. High-resolution three-dimensional aortic magnetic resonance angiography and quantitative vessel wall characterization of different atherosclerotic stages in a rabbit model. *Invest Radiol*. 2007;42:614–621.
28. Phinikaridou A, Ruberg FL, Hallock KJ, Qiao Y, Hua N, Viereck J, Hamilton JA. *In vivo* detection of vulnerable atherosclerotic plaque by MRI in a rabbit model. *Circ Cardiovasc Imaging*. 2010;3:323–332.
29. Markl M, Harloff A, Bley TA, Zaitsev M, Jung B, Weigang E, Langer M, Hennig J, Frydrychowicz A. Time-resolved 3D MR velocity mapping at 3T: improved navigator-gated assessment of vascular anatomy and blood flow. *J Magn Reson Imaging*. 2007;25:824–831.
30. Harloff A, Albrecht F, Spreer J, Stalder AF, Bock J, Frydrychowicz A, Schöllhorn J, Hetzel A, Schumacher M, Hennig J, Markl M. 3D blood flow characteristics in the carotid artery bifurcation assessed by flow-sensitive 4D MRI at 3T. *Magn Reson Med*. 2009;61:65–74.
31. Constantinides P, Chakravarti RN. Rabbit arterial thrombosis production by systemic procedures. *Arch Pathol*. 1961;72:197–208.
32. Abela GS, Picon PD, Friedl SE, Gebara OC, Miyamoto A, Federman M, Tofler GH, Muller JE. Triggering of plaque disruption and arterial thrombosis in an atherosclerotic rabbit model. *Circulation*. 1995;91:776–784.
33. Phinikaridou A, Hallock KJ, Qiao Y, Hamilton JA. A robust rabbit model of human atherosclerosis and atherothrombosis. *J Lipid Res*. 2009;50:787–797.
34. Johnstone MT, Botnar RM, Perez AS, Stewart R, Quist WC, Hamilton JA, Manning WJ. *In vivo* magnetic resonance imaging of experimental thrombosis in a rabbit model. *Arterioscler Thromb Vasc Biol*. 2001;21:1556–1560.
35. Botnar RM, Perez AS, Witte S, Wiethoff AJ, Laredo J, Hamilton J, Quist W, Parsons EC Jr, Vaidya A, Kolodziej A, Barrett JA, Graham PB, Weisskoff RM, Manning WJ, Johnstone MT. *In vivo* molecular imaging of acute and subacute thrombosis using a fibrin-binding magnetic resonance imaging contrast agent. *Circulation*. 2004;109:2023–2029.
36. Pasterkamp G, Borst C, Gussenhoven EJ, Mali WP, Post MJ, The SH, Reekers JA, van den Berg FG. Remodeling of de novo atherosclerotic lesions in femoral arteries: impact on mechanism of balloon angioplasty. *J Am Coll Cardiol*. 1995;26:422–428.
37. Glagov S, Weisenberg E, Zarins CK, Stankunavicius R, Kolettis GJ. Compensatory enlargement of human atherosclerotic coronary arteries. *N Engl J Med*. 1987;316:1371–1375.
38. Losordo DW, Rosenfield K, Kaufman J, Pieczek A, Isner JM. Focal compensatory enlargement of human arteries in response to progressive atherosclerosis. *In vivo* documentation using intravascular ultrasound. *Circulation*. 1994;89:2570–2577.
39. Kim WY, Stuber M, Börnert P, Kissinger KV, Manning WJ, Botnar RM. Three-dimensional black-blood cardiac magnetic resonance coronary vessel wall imaging detects positive arterial remodeling in patients with nonsignificant coronary artery disease. *Circulation*. 2002;106:296–299.
40. Miao C, Chen S, Macedo R, Lai S, Liu K, Li D, Wasserman BA, Vogel-Claussen J, Vogel-Clausen J, Lima JA, Bluemke DA. Positive remodeling of the coronary arteries detected by magnetic resonance imaging in an asymptomatic population: MESA (Multi-Ethnic Study of Atherosclerosis). *J Am Coll Cardiol*. 2009;53:1708–1715.
41. Stone GW, Maehara A, Lansky AJ, de Bruyne B, Cristea E, Mintz GS, Mehran R, McPherson J, Farhat N, Marso SP, Parise H, Templin B, White R, Zhang Z, Serruys PW; PROSPECT Investigators. A prospective natural-history study of coronary atherosclerosis. *N Engl J Med*. 2011;364:226–235.
42. Calvert PA, Obaid DR, O'Sullivan M, Shapiro LM, McNab D, Densem CG, Schofield PM, Braganza D, Clarke SC, Ray KK, West NE, Bennett MR. Association between IVUS findings and adverse outcomes in patients with coronary artery disease: the VIVA (VH-IVUS in Vulnerable Atherosclerosis) Study. *JACC Cardiovasc Imaging*. 2011;4:894–901.
43. Motoyama S, Sarai M, Harigaya H, Anno H, Inoue K, Hara T, Naruse H, Ishii J, Hishida H, Wong ND, Virmani R, Kondo T, Ozaki Y, Narula J. Computed tomographic angiography characteristics of atherosclerotic plaques subsequently resulting in acute coronary syndrome. *J Am Coll Cardiol*. 2009;54:49–57.
44. Pasterkamp G, Schoneveld AH, Hijnen DJ, de Kleijn DP, Teepen H, van der Wal AC, Borst C. Atherosclerotic arterial remodeling and the localization of macrophages and matrix metalloproteases 1, 2 and 9 in the human coronary artery. *Atherosclerosis*. 2000;150:245–253.
45. Cheng C, Helderman F, Tempel D, Segers D, Hierck B, Poelmann R, van Tol A, Duncker DJ, Robbers-Visser D, Ursem NT, van Haperen R, Wentzel JJ, Gijsen F, van der Steen AF, de Crom R, Krams R. Large variations in absolute wall shear stress levels within one species and between species. *Atherosclerosis*. 2007;195:225–235.
46. Keegan J, Gatehouse PD, Mohiaddin RH, Yang GZ, Firmin DN. Comparison of spiral and FLASH phase velocity mapping, with and without breath-holding, for the assessment of left and right coronary artery blood flow velocity. *J Magn Reson Imaging*. 2004;19:40–49.
47. Hays AG, Hirsch GA, Kelle S, Gerstenblith G, Weiss RG, Stuber M. Noninvasive visualization of coronary artery endothelial function in healthy subjects and in patients with coronary artery disease. *J Am Coll Cardiol*. 2010;56:1657–1665.
48. Willerson JT, Golino P, Eidt J, Campbell WB, Buja LM. Specific platelet mediators and unstable coronary artery lesions. Experimental evidence and potential clinical implications. *Circulation*. 1989;80:198–205.
49. Yang C, Canton G, Yuan C, Ferguson M, Hatsukami TS, Tang D. Advanced human carotid plaque progression correlates positively with flow shear stress using follow-up scan data: an *in vivo* MRI multi-patient 3D FSI study. *J Biomech*. 2010;43:2530–2538.

50. Tang D, Teng Z, Canton G, Yang C, Ferguson M, Huang X, Zheng J, Woodard PK, Yuan C. Sites of rupture in human atherosclerotic carotid plaques are associated with high structural stresses: an *in vivo* MRI-based 3D fluid-structure interaction study. *Stroke*. 2009;40:3258–3263.

51. Teng Z, Canton G, Yuan C, Ferguson M, Yang C, Huang X, Zheng J, Woodard PK, Tang D. 3D critical plaque wall stress is a better predictor of carotid plaque rupture sites than flow shear stress: an *in vivo* MRI-based 3D FSI study. *J Biomech Eng*. 2010;132:031007.

CLINICAL PERSPECTIVE

Local hemodynamic factors, particularly low endothelial shear stress, which can only be measured in an in vivo setting, play a crucial role in the formation and progression of the complex disease of atherosclerosis. Our findings demonstrate that low endothelial shear stress is associated with plaque burden, positive vascular remodeling, and plaque disruption in a rabbit model. Noninvasive MRI assessment of endothelial shear stress together with plaque morphology characteristics, in a single examination, offers a comprehensive methodology for monitoring plaque progression, localizing high-risk/vulnerable plaque, and assessing the effect of interventions that aim in plaque regression and stabilization. Early identification of high-risk/vulnerable before acute cardiovascular events will provide enhanced decision making and might improve patient management by allowing prompt aggressive interventions that aim to stabilize plaque.

Circulation
Cardiovascular Imaging

Regions of Low Endothelial Shear Stress Colocalize With Positive Vascular Remodeling and Atherosclerotic Plaque Disruption: An In Vivo Magnetic Resonance Imaging Study

Alkystis Phinikaridou, Ning Hua, Tuan Pham and James A. Hamilton

Circ Cardiovasc Imaging. 2013;6:302-310; originally published online January 28, 2013;
doi: 10.1161/CIRCIMAGING.112.000176
Circulation: Cardiovascular Imaging is published by the American Heart Association, 7272 Greenville Avenue, Dallas, TX 75231

Print ISSN: 1941-9651. Online ISSN: 1942-0080